

Article

Sulfide Formation as a Result of Sulfate Subduction into Silicate Mantle (Experimental Modeling under High P,T-Parameters)

Yuliya Bataleva ^{1,2,*} , Yuri Palyanov ^{1,2} and Yuri Borzdov ^{1,2}

¹ Sobolev Institute of Geology and Mineralogy, Siberian Branch of Russian Academy of Sciences, Koptyug ave 3, 630090 Novosibirsk, Russia; palyanov@igm.nsc.ru (Y.P.); borzdov60@mail.ru (Y.B.)

² Department of Geology and Geophysics, Novosibirsk State University, Pirogova str 2, 630090 Novosibirsk, Russia

* Correspondence: bataleva@igm.nsc.ru; Tel.: +7-3832-330-80-43

Received: 25 June 2018; Accepted: 23 August 2018; Published: 29 August 2018



Abstract: Ca,Mg-sulfates are subduction-related sources of oxidized S-rich fluid under lithospheric mantle P,T-parameters. Experimental study, aimed at the modeling of scenarios of S-rich fluid generation as a result of desulfation and subsequent sulfide formation, was performed using a multi-anvil high-pressure apparatus. Experiments were carried out in the Fe,Ni-olivine–anhydrite–C and Fe,Ni-olivine–Mg-sulfate–C systems ($P = 6.3$ GPa, T of 1050 and 1450 °C, $t = 23$ –60 h). At 1050 °C, the interaction in the olivine–anhydrite–C system leads to the formation of olivine + diopside + pyrrhotite assemblage and at 1450 °C leads to the generation of immiscible silicate-oxide and sulfide melts. Desulfation of this system results in the formation of S-rich reduced fluid via the reaction $\text{olivine} + \text{anhydrite} + \text{C} \rightarrow \text{diopside} + \text{S} + \text{CO}_2$. This fluid is found to be a medium for the recrystallization of olivine, extraction of Fe and Ni, and subsequent crystallization of Fe,Ni-sulfides (i.e., olivine sulfidation). At 1450 °C in the Ca-free system, the generation of carbonate-silicate and Fe,Ni-sulfide melts occurs. Formation of the carbonate component of the melt occurs via the reaction $\text{Mg-sulfate} + \text{C} \rightarrow \text{magnesite} + \text{S}$. It is experimentally shown that the olivine-sulfate interaction can result in mantle sulfide formation and generation of potential mantle metasomatic agents—S- and CO₂-dominated fluids, silicate-oxide melt, or carbonate-silicate melt.

Keywords: sulfate; S-rich fluid; sulfide; sulfidation; desulfation; high-pressure experiment; subduction; mantle metasomatism; lithospheric mantle

1. Introduction

Sulfur, hydrogen, oxygen, and carbon are the major magmatic volatiles in the Earth's mantle and crust. Being a redox-sensitive element, sulfur can exist in reduced form (S^{2-} or S) as sulfides or native sulfur, sulfide melts or reduced fluid, intermediate form (S^{4+}) as an SO₂-component of erupted melts and in oxidized form (S^{6+}) as sulfates, oxidized fluids, or dissolved in silicate melts [1–5]. According to modern concepts, subduction processes play a key role in the transport of S in deep zones of the Earth and are intimately linked to the global geochemical cycle of sulfur, the genesis of arc-related sulfide ore deposits, and the long-term mantle redox evolution [3,6–9]. Existing data demonstrate that only 15–30% of sulfur, transported into the mantle with a subducted slab is released to the atmosphere via magmatic degassing at arcs [7]. Thus, most of the sulfur, which is retained in the down-going slab, either interacts with upper mantle rocks or is recycled to the deep mantle. The heterogeneity of the Earth's mantle as well as redox- and compositional contrast of slab and lithospheric mantle rocks results in numerous scenarios of sulfur behavior in the course of the subduction processes.

Calcium and magnesium sulfates (CaSO_4 and MgSO_4), being the most abundant sulfur-bearing minerals in the Earth's crust, are expected to play a principal role in recycling of oxidized form of sulfur into the deep mantle under subduction settings. There are two lines of direct evidence, demonstrating the possibility of sulfate subduction to the upper mantle depths, particularly (1) findings of anhydrite (CaSO_4) as inclusions in diamonds, in assemblages with coesite [10] and CaCO_3 [10,11], and (2) discovery of similarity of the $\delta^{34}\text{S}$ values of pyrite in eclogite with those of seawater-derived sulfates [12]. Experimental studies of anhydrite structural transitions under high pressure demonstrate that this mineral is stable under high-pressure, high-temperature (HPHT) conditions and does not decompose or melt up to 85 GPa [13–17].

It is known that sulfate stability under mantle conditions can be affected by the sulfur and oxygen fugacities and compositions of the host rock, as well as interactions with the interstitial fluid or melt. The recent experimental studies at variable oxygen fugacity [8,18] showed that anhydrite in the dehydrated slab below the region of formation of arc magmas may efficiently be recycled into the deep mantle. Thermodynamic calculations [3,9] suggest that anhydrite under high pressures should dominantly dissolve into fluids released across the transition from blueschist to eclogite facies, and enrich those fluids with SO_3 , SO_2 , S, HSO_4^- , or H_2S . The main process that results in the decomposition of sulfate with S-rich fluid formation under crustal conditions is desulfation which can occur at the interaction of anhydrite or other sulfates with carbon-bearing brines, resulting in the formation of carbonates and elemental sulfur. A recent investigation of S-bearing species in kimberlites demonstrates that the infiltration of brines into kimberlite can dissolve magmatic sulfates and initiate serpentinization accompanied by sulfidation of olivine [5]. Possible participation of sulfur (sulfide or S form) in the processes of diamond genesis was proposed in [19]. Diamond synthesis in the sulfur-carbon system was demonstrated experimentally [20–22].

Despite the growing interest in this area of research and a number of theoretical and experimental studies, the fate of subducted S-bearing species under high pressures and high temperatures is still poorly known. The most probable reactions involving S-bearing slab minerals, down-going into the silicate mantle, are the interactions of sulfate with silicates as well as carbon-bearing brines. Pioneering experimental work [23] demonstrated that sulfur readily reacts with many of the rock-forming silicates by sulfidation reactions. Recently, we have experimentally investigated these reactions involving olivine and subduction-related reduced S-species, such as S-rich fluid/melt, pyrite, and sulfide melt under high pressures and high temperatures [24]. Here, we report the results of the experimental modeling of interactions of natural Mg,Fe,Ni-olivine with anhydrite and Mg-sulfate (subduction-related oxidized S-species), which are sources of oxidized S-rich fluid under lithospheric mantle P,T-parameters. The main goal of the present study is to propose scenarios of desulfation, oxidized S-rich fluid generation, olivine-S-rich fluid interaction, and evaluate the possibility of sulfide formation via this interaction.

2. Materials and Methods

Experimental studies of the olivine-sulfate interactions were performed in the olivine–anhydrite–C ($\text{Mg}_{1.84}\text{Fe}_{0.14}\text{Ni}_{0.02}\text{SiO}_4\text{–CaSO}_4\text{–C}$) and olivine–Mg-sulfate–C ($\text{Mg}_{1.84}\text{Fe}_{0.14}\text{Ni}_{0.02}\text{SiO}_4\text{–MgSO}_4\text{–C}$) systems at 6.3 GPa, and temperatures of 1050 and 1450 °C, for 23 to 60 h using a multi-anvil high-pressure apparatus of a “split-sphere” type. Details on the pressure and temperature calibration, as well as high-pressure cell schemes, were published previously [25,26]. The starting materials were natural specimens of Fe,Ni-bearing forsterite (spinel lherzolite xenolith from kimberlite of the Udachnaya pipe, Yakutia, Russia), and powders of chemically pure anhydrite and Mg-sulfate (99.99%). Sulfates were preliminary heated at 250 °C for 4 h, to prevent contamination of the experimental charge with water, absorbed from the air. Compositions and proportions of starting materials are shown in Table 1. For every temperature, two or three different concentrations of sulfur (xS) were used. The procedure for the ampoule assembly, in which starting reagents are finely crushed (grain size ~20 μm) and homogenized, was used. The reaction charges were placed in graphite capsules (diameter

of 5 mm, height of 2 mm), which are suitable for HPHT-experiments in sulfur- and iron-bearing systems [27–29]. These graphite capsules provide carbon-saturated conditions, which initiate the decomposition of sulfate (“desulfation”) and S-rich fluid generation. Moreover, graphite acts as an oxygen buffer, providing fO_2 values below CCO (C–CO) buffer equilibrium during the experiments. To examine the effect of carbon-saturated conditions on anhydrite and Mg-sulfate stability under mantle P,T-parameters, two specific experiments were performed (CaSO₄–C and MgSO₄–C systems, P = 6.3 GPa, T = 1450 °C, t = 2 h); it was established, that the sulfate-carbon interaction resulted in the formation of carbonate (solid or melt) and elemental sulfur (melt), see Table 2.

Table 1. Composition of initial olivine, sulfates, and bulk compositions of the systems (wt %).

Phase or System	xS, mol %	Mass Concentrations, wt %						Total
		SiO ₂	FeO	MgO	CaO	NiO	SO ₃	
Olivine	-	41.05	9.25	49.25	-	0.45	-	100.0
Anhydrite	-	-	-	-	46.7	-	53.3	100.0
Magnesium sulfate	-	-	-	38.5	-	-	61.5	100.0
Olivine-anhydrite-C system	2	40.5	9.1	48.1	0.9	0.4	1.0	100.0
	5	39.4	8.8	46.7	2.2	0.4	2.5	100.0
Olivine-magnesium sulfate-C system	5	39.6	8.9	48.6	-	0.4	2.5	100.0
	10	37.9	8.5	48.2	-	0.4	5.0	100.0

Table 2. Experimental conditions and results.

Run N	T, °C	t, h	System	xS, mol %	Final Phases
933-2	1050	60	Ol–CaSO ₄ –C	2	Ol _R , Cpx, Po
933-5	1050	60	Ol–CaSO ₄ –C	5	Ol _R , Cpx, Po
934-2	1450	23	Ol–CaSO ₄ –C	2	Ol _R , L _{sulf} , L _{sil-ox}
934-5	1450	23	Ol–CaSO ₄ –C	5	Ol _R , L _{sulf} , L _{sil-ox}
1809-5	1450	40	Ol–MgSO ₄ –C	5	Ol _R , L _{sulf} , L _{carb-sil}
1809-10	1450	40	Ol–MgSO ₄ –C	10	Ol _R , L _{sulf} , L _{carb-sil}
571-M	1450	2	MgSO ₄ –C	-	Ms, L _S
571-C	1450	2	CaSO ₄ –C	-	L _{carb} , L _S

Ol—olivine, Ol_R—recrystallized olivine, Cpx—clinopyroxene, Po—pyrrhotite, L_{sulf}—sulfide melt, L_{carb-sil}—carbonate-silicate melt; L_{carb}—carbonate melt, L_S—sulfur melt, Ms—magnesite, xS—molar concentration of sulfur in the system.

The lower temperature of 1050 °C at 6.3 GPa was chosen according to P-T estimates of the formation of anhydrite-bearing diamond [10,11,30], see Figure 1. The higher temperature of 1450 °C at 6.3 GPa corresponds to the Ni-rich pyrrhotite melting under carbon-saturated conditions, see Figure 1. Following the experiments, phase identification of samples, analysis of phase relations, and measurements of energy dispersive spectra (EDS) of various phases were performed using a TESCAN MIRA 3 LMU scanning electron microscope (TESCAN, Brno, Czech Republic).

The chemical composition of mineral phases was analyzed using a Cameca Camebax-Micro microprobe (CAMECA, Gennevilliers, France). For the microprobe and EDS analysis, samples in the form of polished sections were prepared. An accelerating voltage of 20 kV and a probe current of 20 nA were used for all the analyses of crystalline phases. For the quenched melt, the accelerating voltage was lowered to 15 kV and the probe current to 10 nA. For the bulk of the analyses, a focused beam (d = 2–4 μm) for silicate and sulfide crystalline phases and a beam diameter of 20–100 μm for the quenched melt were used. Peak counting time was 60 s. Standards, used for the analyses of quenched sulfide melt were natural pyrite, pyrrhotite, and pentlandite. Analytical studies were performed at the Center for Collective Use of Multi-element and Isotopic Analysis of the Siberian Branch of the Russian Academy of Sciences.

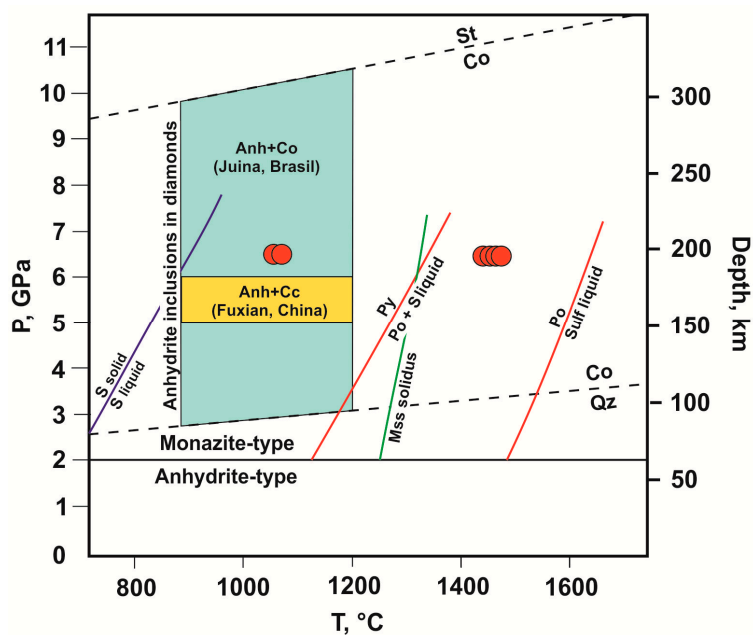


Figure 1. P-T diagram with experimental parameters (circles), line of structural transition of anhydrite [17], estimated field of the formation of diamonds with anhydrite inclusions [10,11,30], and experimentally determined melting curves of sulfur, pyrrhotite, and Mss and decomposition of pyrite [31–33]. **Sulf**—sulfide, **Po**—pyrrhotite, **Py**—pyrite, **Mss**—monosulfide solid solution ($\text{Fe}_{0.69}\text{Ni}_{0.23}\text{Cu}_{0.01}\text{S}_{1.00}$), **Anh**—anhydrite, **Co**—coesite, **St**—stishovite, **Qz**—quartz, **Cc**—calcite.

3. Results

3.1. Interaction in the Olivine–Anhydrite–C System

Experimental parameters and results are shown in Table 2. At a temperature of 1050 °C, 60 h, and $xS = 2\text{--}5$ mol %, a polycrystalline olivine aggregate with newly formed clinopyroxene and pyrrhotite in the interstices is formed, see Figure 2a,b and Figure 3a,b. The amount of these newly formed phases increases as the initial sulfur concentration in the system increases, as shown in Figure 2. Clinopyroxene and pyrrhotite occur as inclusions in olivine, see Figure 3b. The initial sulfate is absent in the samples after the experiments.

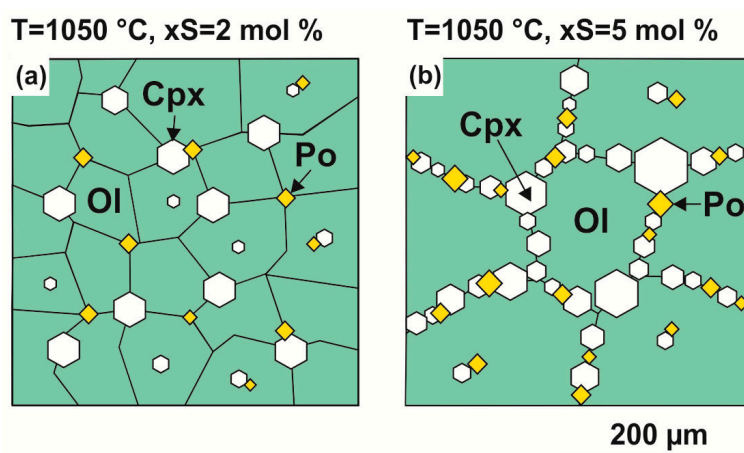


Figure 2. Schematic images of experimental products in olivine–anhydrite–C system, at 1050 °C, $xS = 2$ mol % (a) and $xS = 5$ mol % (b); **Ol**—olivine, **Cpx**—clinopyroxene, **Po**—pyrrhotite.

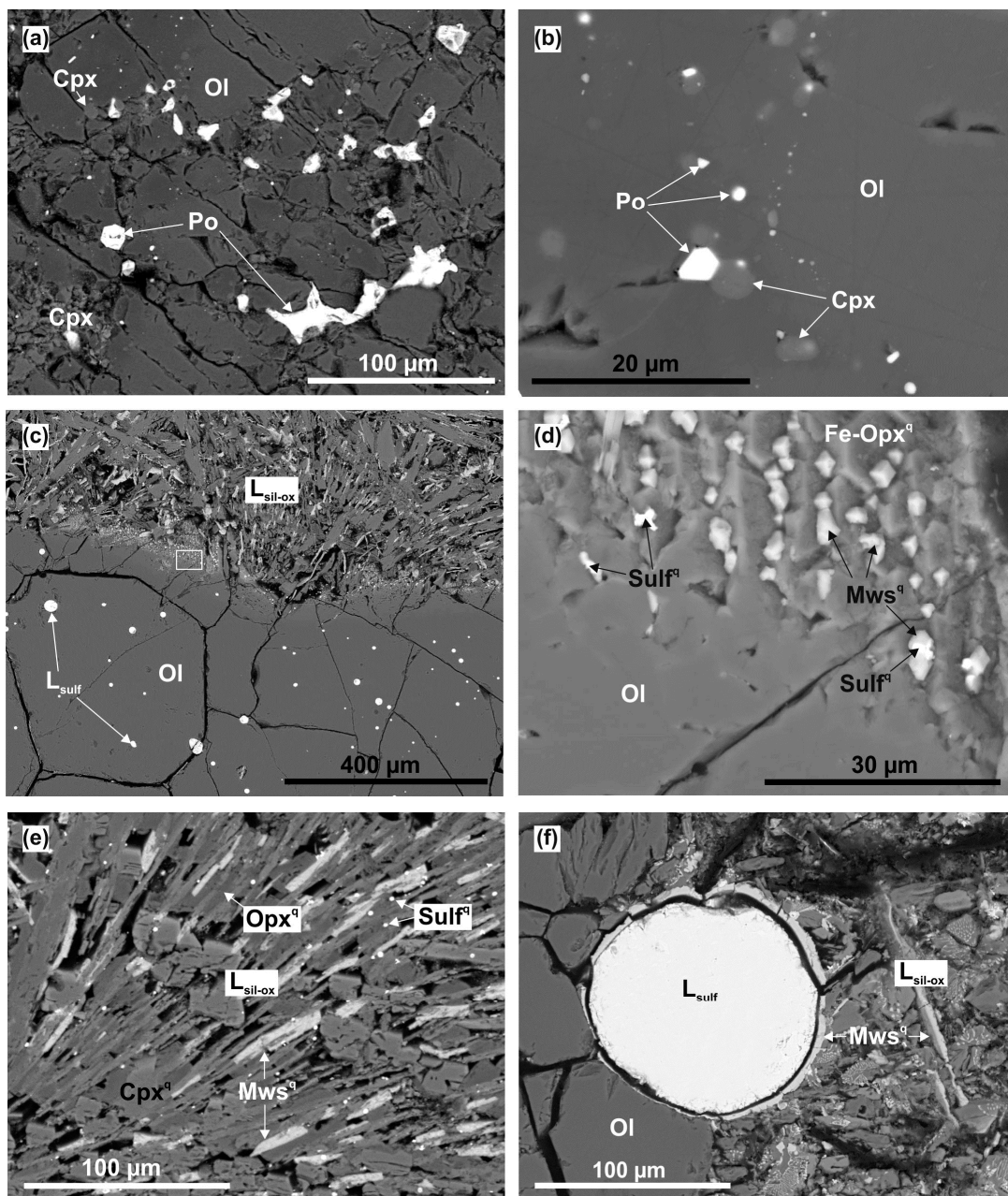


Figure 3. Scanning electron microscopy (SEM) images of polished fragments of the samples after experiments in olivine–anhydrite–C system, (a–d) 1050 °C, $xS = 2$ mol %, (e–f) 1450 °C, $xS = 2$ mol %: (a) Polycrystalline aggregate of recrystallized olivine with clinopyroxene and pyrrhotite in interstices; (b) inclusions of clinopyroxene and pyrrhotite in recrystallized olivine; (c) recrystallized olivine with sulfide melt inclusions, at the contact with the quenched silicate-oxide melt; (d) enlarged fragment of Figure 3c, quenched magnesiowüstite and ferrous orthopyroxene at the contact with olivine; (e) structure of the quenched silicate-oxide melt, consisted of pyroxenes and magnesiowüstite; (f) a contact of the quenched sulfide melt spherule with the quenched silicate-oxide melt, and a rim of magnesiowüstite between them; **Ol**—olivine, **Cpx**—clinopyroxene, **Po**—pyrrhotite, **Sulf**—sulfide, **L_{sil-ox}**—silicate-oxide melt, **L_{sulf}**—sulfide melt, **Opx**—orthopyroxene, **Mws**—magnesiowüstite, ^q—quenched phase.

Olivine demonstrates recrystallization features, involving; (1) increase in the crystal size from the initial 20 μm to 150 μm ($xS = 2$ mol %) and 350 μm ($xS = 5$ mol %); (2) formation of inclusions;

and (3) zonal structure of crystals, with relicts of the initial olivine in cores and lower Fe and Ni rims. A similar decrease in FeO and NiO and an increase in MgO towards the rims of olivine are considered as the main signs of olivine sulfidation in nature [34]. The formation of zonal olivine crystals occurs only at $xS = 2$ mol %. The composition of the core and rim zones of this olivine is shown in Figure 4a. On average, the composition of the recrystallized olivine is characterized by a decrease in the FeO concentration (relative to the initial 9.3 wt %) to 7.5 wt % ($xS = 2$ wt %) and 8.0 wt % ($xS = 5$ wt %), as well as a negligible CaO content, see Table 3. Newly formed clinopyroxene compositions correspond to $Mg_{1.13}Ca_{0.85}Fe_{0.06}Si_2O_6$ ($xS = 2$ wt %) and $Mg_{1.12}Ca_{0.75}Fe_{0.09}Si_2O_6$ ($xS = 5$ wt %), which are identical to included (size 1–7 μm) and interstitial (crystal size 3–15 μm) pyroxenes. Pyrrhotite has an admixture of Ni of 6.3 wt % ($xS = 2$ mol %) and 11 wt % ($xS = 5$ wt %), see Figure 5a and Table 4.

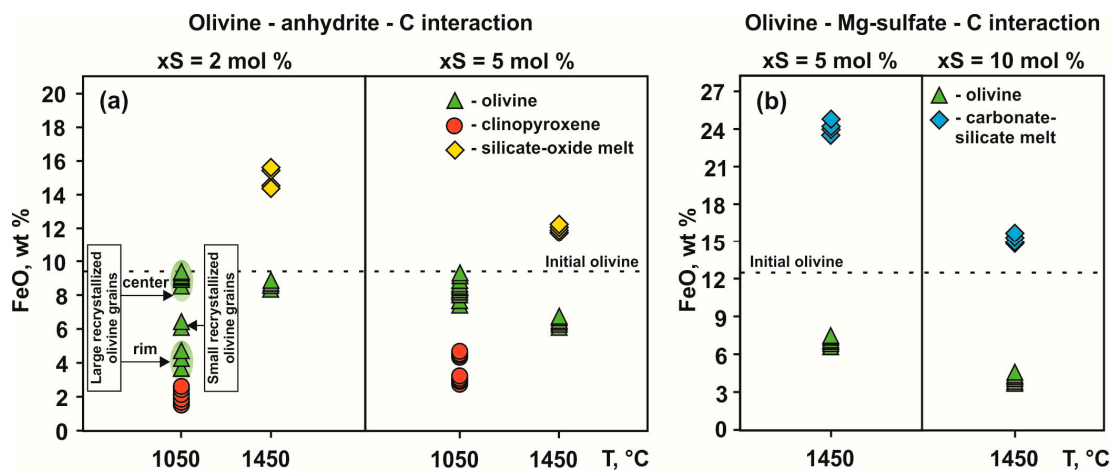


Figure 4. Temperature and sulfur content (xS) dependencies of FeO concentrations in silicates and silicate-oxide melts.

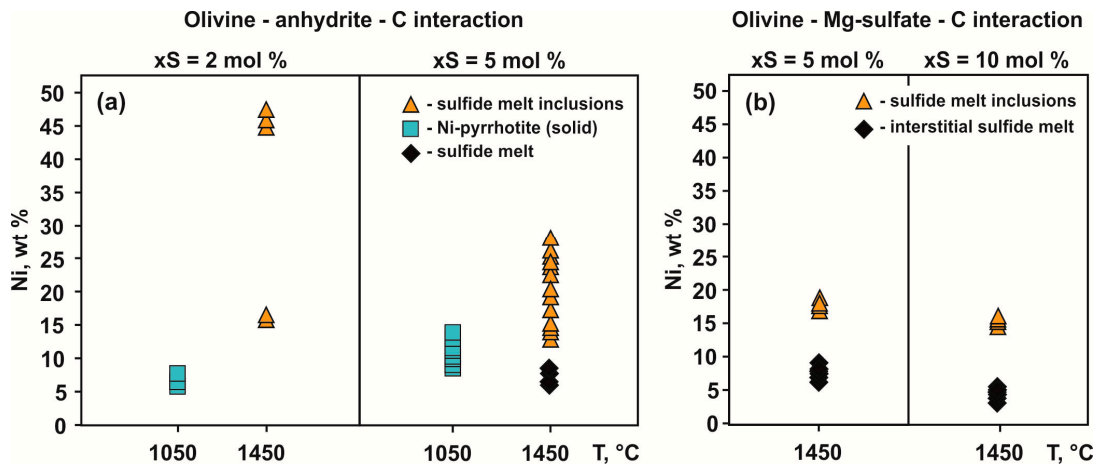


Figure 5. Temperature and sulfur content (xS) dependencies of Ni concentrations in sulfides and sulfide melts.

Table 3. Compositions of silicates, silicate-oxide and carbonate-silicate melts.

Run N	T, °C	xS,mol %	Phase	N _A	Composition, wt %							n(O)	Cations per Formula Unit						
					SiO ₂	FeO	MgO	CaO	NiO	CO ₂	Total		Si	Fe	Mg	Ca	Ni	Sum	
Ol–CaSO ₄ –C system																			
933-2	1050	2	Ol	14	41.2 ₍₆₎	7.5 ₍₂₈₎	50.0 ₍₅₄₎	1.0 ₍₇₎	0.2 ₍₂₎	-	99.9 ₍₄₎	4	1.00 ₍₁₎	0.15 ₍₆₎	1.82 ₍₁₇₎	0.03 ₍₂₎	-	2.99 ₍₁₎	
933-5	1050	5	Cpx	8	54.8 ₍₁₄₎	2.1 ₍₅₎	20.9 ₍₃₉₎	22.0 ₍₂₈₎	0.1 ₍₁₎	-	99.9 ₍₃₎	6	1.98 ₍₅₎	0.06 ₍₂₎	1.13 ₍₂₀₎	0.85 ₍₁₁₎	-	4.02 ₍₂₎	
			Ol	27	40.7 ₍₄₎	8.6 ₍₆₎	49.7 ₍₇₎	0.2 ₍₂₎	0.3 ₍₁₎	-	99.6 ₍₃₎	4	1.00 ₍₁₉₎	0.17 ₍₂₎	1.82 ₍₃₎	-	0.01 ₍₀₎	3.00 ₍₄₎	
934-2	1450	2	Cpx	10	56.5 ₍₅₎	3.1 ₍₆₎	23.6 ₍₆₆₎	16.2 ₍₇₈₎	0.1 ₍₁₎	-	99.5 ₍₃₎	6	2.02 ₍₁₎	0.09 ₍₁₎	1.12 ₍₄₎	0.75 ₍₃₎	-	3.98 ₍₁₎	
			Ol	9	41.1 ₍₁₎	8.4 ₍₁₎	50.6 ₍₃₎	0.2 ₍₀₎	-	-	100.3 ₍₃₎	4	0.99 ₍₀₎	0.17 ₍₀₎	1.84 ₍₁₎	0.01 ₍₀₎	-	3.01 ₍₀₎	
934-5	1450	5	Liq1	19	41.8 ₍₈₎	14.6 ₍₉₎	29.6 ₍₄₎	13.6 ₍₁₁₎	-	-	99.6 ₍₅₎	-	-	-	-	-	-	-	
			Ol	8	41.7 ₍₃₎	6.1 ₍₁₎	51.6 ₍₂₎	0.2 ₍₁₎	-	-	99.5 ₍₃₎	4	1.00 ₍₀₎	0.12 ₍₀₎	1.86 ₍₁₎	0.01 ₍₀₎	-	3.00 ₍₀₎	
			Liq1	15	38.0 ₍₁₎	12.8 ₍₁₎	22.2 ₍₁₈₎	26.4 ₍₂₀₎	-	-	99.4 ₍₃₎	-	-	-	-	-	-	-	
Ol–MgSO ₄ –C system																			
1809-5	1450	5	Ol	16	41.2 ₍₂₎	6.7 ₍₁₎	51.6 ₍₃₎	-	0.1 ₍₁₎	-	99.6 ₍₃₎	4	1.00 ₍₀₎	0.14 ₍₀₎	1.87 ₍₁₎	-	-	3.00 ₍₀₎	
			Fms ^q	4	-	5.2 ₍₂₎	42.3 ₍₂₎	0.9 ₍₁₎	-	51.6 ₍₄₎	100	3	-	0.06 ₍₀₎	0.91 ₍₀₎	0.01 ₍₀₎	-	0.98 ₍₀₎	
			Opx ^q	10	57.6 ₍₃₎	6.9 ₍₂₎	35.4 ₍₃₎	-	-	-	-	99.9	6	1.99 ₍₀₎	0.20 ₍₀₎	1.83 ₍₀₎	-	-	4.01 ₍₀₎
			Liq2	20	32.0 ₍₂₀₎	24.1 ₍₄₈₎	36.9 ₍₃₁₎	-	-	6.5 ₍₅₎	99.5 ₍₂₎	-	-	-	-	-	-	-	-
1809-10	1450	10	Ol	12	41.8 ₍₂₎	4.4 ₍₈₎	53.4 ₍₆₎	-	-	-	99.8 ₍₃₎	4	1.00 ₍₀₎	0.09 ₍₂₎	1.91 ₍₂₎	-	-	3.00 ₍₀₎	
			Liq2	21	31.7 ₍₃₆₎	15.2 ₍₇₇₎	44.3 ₍₇₈₎	-	-	8.1 ₍₁₎	99.3 ₍₃₎	-	-	-	-	-	-	-	

Ol—olivine, Cpx—clinopyroxene, Opx^q—quenched orthopyroxene, Fms^q—quenched ferromagnesite, Liq1—silicate-oxide melt, Liq2—carbonate-silicate melt, N_A—number of analyses, n(O)—number of oxygen atoms; The values in parentheses are one sigma errors of the means based on replicate electron microprobe analyses reported as least units cited.

Table 4. Compositions of sulfides.

Run N	T, °C	xS, mol %	Phase	N _A	Composition, wt %				n(S)	Cations per Formula Unit	
					Fe	Ni	S	Total		Fe	Ni
Ol–CaSO ₄ –C system											
933-2	1050	2	Ni-Po	9	56 ₍₃₎	6.3 ₍₂₇₎	37.0 ₍₃₎	99.6	1	0.87 ₍₅₎	0.09 ₍₄₎
933-5	1050	5	Ni-Po	8	50 ₍₂₎	11 ₍₂₎	38.4 ₍₁₀₎	99.3	1	0.74 ₍₆₎	0.16 ₍₃₎
934-2	1450	2	Liq ^A	9	41 ₍₁₁₎	24 ₍₁₄₎	35 ₍₃₎	99.5	1	0.66 ₍₁₃₎	0.4 ₍₃₎
934-5	1450	5	Liq ^A	16	45 ₍₉₎	21 ₍₁₀₎	33 ₍₁₎	99.6	1	0.78 ₍₁₄₎	0.34 ₍₁₉₎
			Liq ^B	14	56 ₍₁₎	7 ₍₁₎	36.0 ₍₇₎	99.5	1	0.89 ₍₄₎	0.12 ₍₁₎
Ol–MgSO ₄ –C system											
1809-5	1450	5	Liq ^A	11	46.1 ₍₈₎	17 ₍₁₎	36.4 ₍₁₎	99.7	1	0.72 ₍₁₎	0.26 ₍₂₎
			Liq ^B	10	53.1 ₍₅₎	8.5 ₍₄₎	37.9 ₍₂₎	99.5	1	0.80 ₍₁₎	0.12 ₍₁₎
1809-10	1450	10	Liq ^A	14	47 ₍₁₎	16 ₍₂₎	36.5 ₍₂₎	99.6	1	0.74 ₍₂₎	0.24 ₍₃₎
			Liq ^B	10	56.6 ₍₄₎	5.5 ₍₄₎	37.5 ₍₄₎	99.5	1	0.86 ₍₁₎	0.08 ₍₁₎

Ni-Po—Ni-bearing pyrrhotite, Liq^A—sulfide melt from interstices or inclusions, Liq^B—sulfide melt drops from quenched silicate-oxide or carbonate-silicate melt; the values in parentheses are one sigma errors of the means based on replicate electron microprobe analyses reported as least units cited.

At 1450 °C, $t = 23$ h, and $xS = 2$ mol %, formation of a polycrystalline aggregate of olivine (crystal size of 100–400 μm) with inclusions of the quenched sulfide melt, in addition to a large pool of segregated quenched silicate-oxide melt, shown in Figures 3c–e and 6a, occur. At higher sulfur contents (5 mol %), the grain size of the recrystallized olivine increases to 400–700 μm , and the sulfide melt is present not only in inclusions but also in interstices. Its drops are also located as quenched silicate-oxide melt, as shown in Figures 3f and 6b.

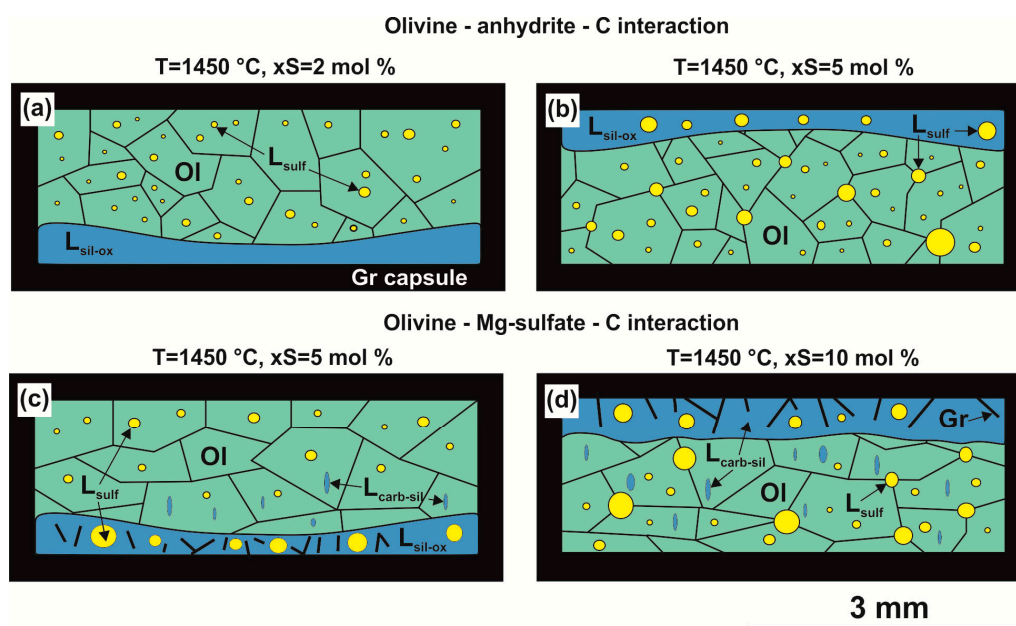


Figure 6. Schematic images of experimental results at 1450 °C in olivine-anhydrite-C system at $xS = 2$ mol % (a) and $xS = 5$ mol % (b) and in Mg-sulfate–olivine system at $xS = 5$ mol % (c) and $xS = 10$ mol % (d); OI—olivine, Gr—graphite, L_{sulf}—sulfide melt, L_{sil-ox}—silicate-oxide melt.

Magnesiowustite rims form between immiscible quenched melts and are shown in Figure 3f. Olivine is homogeneous in composition, it shows a decrease in the FeO concentration (relative to the initial) to 8.4 wt % ($xS = 2$ mol %) and 6.1 wt % ($xS = 5$ mol %), as shown in Figure 4a. The composition of sulfide melt in inclusions at $xS = 2$ mol % corresponds to $\text{Fe}_{0.53-0.79}\text{Ni}_{0.21-0.47}\text{S}$, and is

characterized by wide variations in Ni content (10–38 wt %). At $xS = 5$ mol %, the composition of the sulfide melt from the interstices of the polycrystalline olivine aggregate and the inclusions, corresponds to $Fe_{0.64-0.92}Ni_{0.15-0.53}S$; the sulfide melt drops originating from the silicate-oxide melt have lower Ni content, with a composition of $Fe_{0.85-0.93}Ni_{0.11-0.13}S$, see Figure 5a. The quenched aggregate of the silicate-oxide melt is represented by micro dendrites of clinopyroxene, orthopyroxene, and magnesiowüstite, as well as submicron sulfide species, as shown in Figure 3e. The bulk composition of this melt at $xS = 2$ mol % is characterized by 14.6 wt % FeO and 13.6 wt % CaO concentrations, and at the higher sulfur content in the system—12.8 wt % FeO and 26.4 wt % CaO. At $xS = 2$ mol %, specific quenched aggregates were established at the olivine/silicate-oxide melt contact, see Figure 3c,d.

The analysis of experimental results reveals the main regularities of phase formation in the olivine–anhydrite–C system depending on temperature and sulfur content, controlled by the amount of initial sulfate. It was experimentally established that with an increase in the sulfur content from 2 to 5 mol % in the system (irrespective of temperature), the average size of the olivine crystals increases, FeO and NiO concentrations in olivine decrease, and the number and grain size of the newly formed sulfide and clinopyroxene increase. Depending on the sulfur content in the system, formation of Fe-enriched reaction structures at the contact of olivine with the silicate-oxide melt ($xS = 2$ mol %) or segregation of sulfide melt droplets directly in the silicate-oxide melt ($xS = 5$ mol %) occur. An increase of the temperature of experiments ($xS = \text{const}$) also leads to an increase in the size of the olivine crystals, a decrease in the concentration of iron and nickel therein, as well as to the change of association of the newly formed phases from a clinopyroxene + pyrrhotite to a silicate-oxide melt + sulfide melt.

3.2. Interaction in the Olivine—Mg-sulfate—C System

At 1450 °C and $xS = 5$ mol %, the formation of a polycrystalline olivine aggregate, as well as the carbonate-silicate melt occur, as shown in Figure 7a–d. This melt is presented in the experimental samples as micro-dendritic aggregates of clinopyroxene, orthopyroxene, and magnesite, as shown in Figure 7d. In the quenched aggregate of a carbonate-silicate melt, segregated drops of sulfide melt and graphite crystals are situated as shown in Figure 7a–d,f. Additionally, quenched ferromagnesite and Ni-pyrrhotite are present in the interstices of the polycrystalline olivine aggregate, see Figure 7e. Recrystallized olivine (grain size of ~200–500 μm) contains inclusions of quenched melts—sulfide and carbonate-silicate, see Figure 7a–c.

The composition of the olivine corresponds to $Mg_{1.86}Fe_{0.14}SiO_4$; it demonstrates the complete absence of a nickel impurity, as well as a decrease in the iron concentration to 6.7 wt % relative to the initial concentration. The carbonate-silicate melt that co-exists with olivine is characterized by an FeO content of ~24 wt % and a CO_2 concentration of 6–7 wt %, as shown in Table 3 and Figure 4b. The composition of sulfide melt in the inclusions and interstices of the polycrystalline olivine aggregate corresponds to $Fe_{0.70-0.74}Ni_{0.24-0.28}S$, see Table 4 and Figure 5b, and the sulfide droplets in the carbonate-silicate melt are characterized by a composition of $Fe_{0.79-0.81}Ni_{0.11-0.13}S$. At higher sulfur contents (10 mol %), the structure of the experimental sample is generally similar to the above. The FeO content in the olivine is decreased to 4.4 wt %. The carbonate-silicate melt is characterized by FeO content of 15 wt % and CO_2 concentration of 8.5 wt %. The composition of the sulfide melt in inclusions in olivine and in interstices corresponds to $Fe_{0.72-0.76}Ni_{0.21-0.27}S$, see Figure 5b, while drops of sulfide in the carbonate-silicate melt are of the composition, $Fe_{0.85-0.87}Ni_{0.07-0.09}S$. Thus, it has been experimentally demonstrated that the increase in the sulfur concentration in the olivine—Mg-sulfate–C system at a relatively high temperature leads to an increase in the average size of the olivine crystals, a decrease in the concentration of iron and nickel in olivine and in the carbonate-silicate melt, and an increase in the amount of the newly formed sulfide melt.

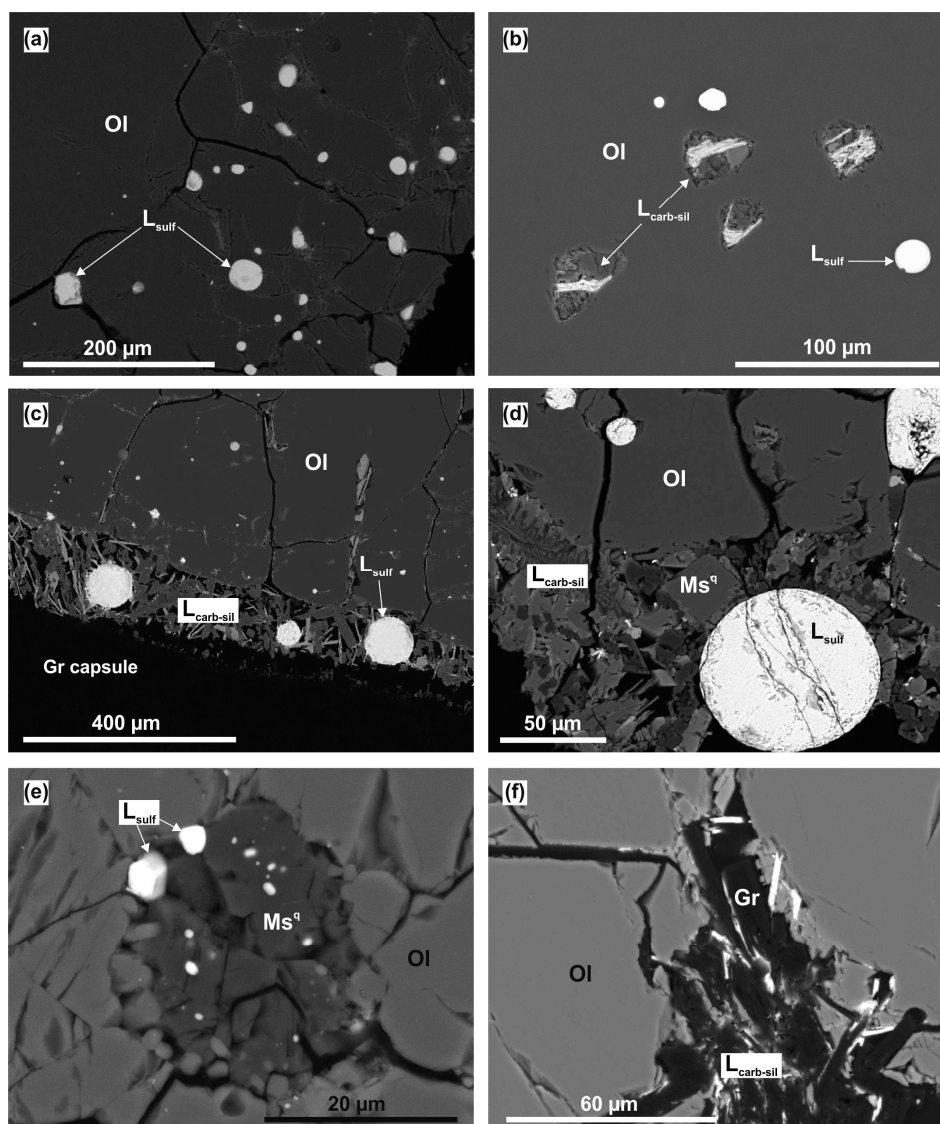


Figure 7. Scanning electron microscopy (SEM) images of polished fragments of the samples after experiments on the Mg-sulfate-olivine system, 1450 °C, xS = 5 mol %: (a) Polycrystalline aggregate of recrystallized olivine with sulfide and silicate-oxide melt in interstitions and inclusions; (b) inclusions of quenched sulfide and silicate-oxide melt in recrystallized olivine; (c,d) recrystallized olivine with inclusions, at the contact with the quenched silicate-oxide and sulfide immiscible melts; (e) aggregate of quenched ferromagnesite and sulfide melt; (f) recrystallized graphite in a quenched carbonate-silicate melt; **Ol**—olivine, **L_{carb-sil}**—carbonate-silicate melt, **L_{sulf}**—sulfide melt, **Ms**—magnesite, **Gr**—graphite, **q**—quenched phase.

4. Discussion

4.1. Reconstruction of Sulfate-Olivine Interaction Processes

The interaction processes in the olivine–anhydrite–C and olivine–Mg-sulfate–C systems are found to proceed via closely interrelated reactions and involving the generation of fluid or melt, recrystallization and crystallization of mineral phases, and the formation of inclusions therein. Given the complexity of the processes, they will be considered separately.

4.1.1. S-Rich Fluid Formation Processes in Olivine–Anhydrite–C System

The most informative experiments in terms of the reconstruction of fluid generation processes are those in the olivine–anhydrite–C system at sub-solidus temperatures, under averaged P,T-parameters estimated for the formation of sulfate inclusions in natural diamonds, see Figure 1. It has been established that the formation of a fluid, that has a direct influence on the phase formation in the system, takes place mainly through the desulfation reaction. This reaction under natural conditions (at high P and T) is thought to be realized by the interaction of Ca,Mg-sulfates with silicates or oxides, and leads to the formation of oxidized SO₃-fluid and enrichment of the associated phases with calcium or magnesium [3]. In our experiments on the olivine–anhydrite–C interaction, desulfation occurs via the scheme $Ol + Anh \rightarrow Di + SO_3$ (1), and results in complete consumption of anhydrite. In this case, CaO, initially contained in the anhydrite, enters diopside, which forms in the interstices of the polycrystalline aggregate of olivine and in the inclusions therein. Under the carbon-saturated conditions, provided by the graphite ampoules, SO₃-fluid is reduced, according to the $2SO_3 + 3C \rightarrow 2S + 3CO_2$ (2) scheme. For a full-scale reconstruction of the fluid generation processes, it should be noted that there is a different understanding of the mechanisms of desulfation in nature. Desulfation is one of the characteristic processes that occur during the formation of infiltration-metasomatic deposits of sulfur in the Earth's crust. It can occur through the interaction of anhydrite (or oxidized SO₂, SO₃-fluid) with organic matter or carbon-bearing brines, and is accompanied by the formation of calcite and elemental sulfur. Moreover, a recent investigation of non-salty kimberlites, demonstrating an increased abundance of sulfides, showed that the infiltration of brines into kimberlites can dissolve magmatic sulfates and initiate serpentinization accompanied by the sulfidation of olivine [5]. The process of desulfation, realized by the interaction of sulfate + C, can also occur at great depths in the mantle, as evidenced by the presence of CaCO₃ in all described inclusions of anhydrite in diamonds [10,11]. Thus, as the main indicator of the realization of the desulfation reaction in carbon-saturated conditions, the formation of carbonate and a phase (mineral, fluid or melt) that bears sulfur in a reduced form can be considered. However, the experiments in the olivine–anhydrite–C system do not produce CaCO₃, but rather CaO in diopside. This result emphasizes the preference of the anhydrite + silicate interaction instead of the anhydrite + graphite under high pressure and temperatures. The formation of a diopside + Ni-pyrrhotite mineral association in inclusions in olivine and in interstices indicates that the reconstructed process of the fluid formation proceeds in stages, as a result of interactions (1) and (2), and not directly by the interaction of anhydrite + C.

4.1.2. Fe,Ni-Sulfide Formation via Olivine Interaction with S-rich Fluid in the Olivine–Anhydrite–C System

In the course of the interaction of Fe,Ni-olivine with S-rich fluid, generated by desulfation, even relatively low concentrations of the intergranular fluid provide conditions for the recrystallization of olivine–partial (1050 °C, xS = 2 mol %) and total (xS = 5 mol %). It was found that during recrystallization, extraction of iron, nickel, and other elements from olivine into intergranular S-rich fluid, results in a fluid that can be denoted as [S-Fe-Ni-O-Si-Mg]_{fluid}. When this fluid, enriched with metals and oxygen due to their extraction from olivine, reaches saturation conditions, formation of Ni-pyrrhotite as a separate phase, enrichment of interstitial clinopyroxene with FeO and MgO, and crystallization of Fe,Ni-poor olivine occur. The bulk of these processes, including olivine recrystallization, Fe and Ni extraction in S-rich fluid, sulfide formation, as well as pyroxene crystallization are realized in the course of olivine sulfidation [23,24,35]. Details on the reconstruction of the olivine sulfidation mechanism (xS = 10 mol %) under mantle P,T-parameters are presented in [24].

4.1.3. The Formation of Silicate-Oxide and Sulfide Melts in the Olivine–Anhydrite–C System

At 1450 °C, the generation of S-rich reduced fluid, recrystallization of olivine in this fluid, and the extraction of metals, accompanied by the formation of sulfide, occurs. In addition to these processes, partial melting leads to the formation of two immiscible melts—the sulfide and silicate-oxide ones.

In the olivine–anhydrite–C system at a sulfur content of 2 mol %, the formation of Ni-rich sulfide melt droplets occur only in the interstices, simultaneously with olivine recrystallization in the intergranular fluid and the subsequent capture of sulfide inclusions. The mechanism of the sulfide melt formation is similar to that of Ni-pyrrhotite crystallization at a lower temperature. However, the formation of submicron Ni-poor pyrrhotite crystals in the quenched silicate-oxide melt indicates that some sulfur is dissolved in this melt. As it is shown in the works on the solubility of sulfur in silicate melts under mantle P,T-parameters [4,36], the highest solubility is characteristic of the “sulfate” form of sulfur (S^{6+}). The “Sulfide” form of sulfur (S^{2-}) is known to be dissolved in the silicate melt as predominantly Fe-S. However, the solubility of “sulfide” sulfur is very low, and when the silicate melts are saturated with S^{2-} , the sulfide component of the melt is segregated [4,36,37]. Analysis of the Fe-rich structures, see Figure 3d, arising at the contact of olivine with the silicate-oxide melt ($xS = 2$ mol %) shows that the olivine recrystallization occurs not only in reduced S-rich fluid, but also in the silicate-oxide melt with dissolved sulfur. As a result of the extraction of iron, nickel, and other elements from olivine into the melt, and the subsequent interaction of Fe and Ni with the dissolved sulfur, Fe-S and Ni-S ligands are formed, that are quenched as submicron pyrrhotite species ($xS = 2$ mol %) or are segregated as large drops of sulfide directly in the silicate-oxide melt ($xS = 5$ mol %). The main indicators of sulfide in the silicate-oxide melt are: (1) The spatial confinement of sulfides to quenched magnesiowüstite, and (2) dramatic differences in the Ni concentration in the interstitial sulfide melt (high-nickel) and in the silicate-oxide melt (low-nickel), see Figure 5a.

4.1.4. The Formation of Carbonate-Silicate and Sulfide Melts in the Olivine–Mg-Sulfate–C System

The presence of quenched ferromagnesite and Ni-pyrrhotite in the interstices of a polycrystalline aggregate of olivine and the formation of a carbonate-bearing melt indicate that the desulfation scenario in the olivine–Mg-sulfate–C system differs entirely from that in the olivine–anhydrite–C system. In this case, the initiation of partial melting and the formation of the carbonate component of the melt occurs as a result of the desulfation reaction according to the scheme $Mg\text{-sulfate} + C \rightarrow \text{magnesite} + S_{\text{fluid}}$. Reduced sulfur in the interstitial fluid causes olivine sulfidation–extraction of iron, nickel, and other elements into the fluid and formation of Ni-pyrrhotite, as well as enrichment of magnesite with FeO. The newly formed sulfide undergoes melting under the P,T-parameters of the experiments, and in the process of recrystallization of olivine, the inclusions of the sulfide melt are trapped. At the same time, sufficiently high sulfur concentrations in the system (5 and 10 mol %) lead to complete recrystallization of olivine and the formation of orthopyroxene—a product of olivine sulfidation.

As noted above, the capture of inclusions of the sulfide melt occurs directly from the interstitial spaces during the recrystallization of olivine. In this case, the newly formed ferromagnesite and Fe-orthopyroxene in the presence of a reduced sulfur fluid undergo partial melting and form droplets of carbonate-silicate melt with a small amount of dissolved sulfur. During the experiment, the droplets of the carbonate-silicate melt segregate and move from the interstices into a single melt pool. Inclusions of carbonate-silicate melt in the olivine indicate that its recrystallization is realized not only in the reduced sulfur fluid, but also in the carbonate-silicate melt containing dissolved sulfur. The direct result of this recrystallization and extraction of Fe, Ni, and other elements from olivine into the melt is the formation of droplets of sulfide in the carbonate-silicate melt. Most probably, recrystallization of graphite in carbonate-silicate melt proceeds via the redox reaction of a sulfide and a carbonate-bearing melt under carbon-saturated conditions [29,38,39].

4.2. Scenarios of Ca,Mg-Sulfates Interaction with Olivine Under High P,T-Conditions: Implications to Mantle Sulfide, Silicate and Carbonate Formation

During subduction, the main fluid-generating processes are supposed to be dehydration (water-releasing process with hydrous minerals decomposition), decarbonation (formation of CO_2 -fluid with carbonates decomposition), and desulfation (formation of SO_3 -fluid with sulfates decomposition). P,T-parameters of the realization of these processes vary widely and depend on many factors, such

as fO_2 , fS_2 , and environment composition [9,18,40]. In the studies on the behavior of sulfur-bearing phases under subduction conditions, sulfate interactions with carbon-rich brines, reduced H-rich fluids, silicates, and silicate melts are proposed as specific processes for the formation of S-rich fluid. Results of the present study demonstrate that the interaction of Ca,Mg-sulfates with Fe,Ni-bearing forsterite (under carbon-saturated conditions) can be considered as a simplified model of these processes occurring during the subduction of oxidized crustal material into silicate mantle. However, revealed scenarios of the formation of mantle sulfides, silicates, carbonates and melts of various compositions are also applicable to more complex natural systems.

It is established that, in the process of the subduction of anhydrite into a silicate mantle, desulfation occurs as a result of its interaction with olivine, and leads to the generation of an oxidized SO_3 -fluid and crystallization of a diopside, or the formation of a silicate-oxide melt enriched in calcium. In this case, despite carbon-saturated conditions, anhydrite does not participate in carbonate-producing reactions with C directly. In the presence of graphite, the SO_3 -fluid is reduced to S (as fluid), and this process is accompanied by the formation of the CO_2 -fluid. Subduction of Mg-sulfate into the silicate mantle under carbon-saturated conditions leads to the formation of carbonate (or carbonate-silicate melt) and reduced S-rich fluid. As a result of the interaction of this fluid with Fe,Ni-bearing forsterite, olivine is sulfidized, leading to the crystallization of Fe, Ni-sulfides, or the formation of a sulfide melt.

5. Conclusions

It is found that at a relatively low temperature (1050 °C), interaction in the Fe,Ni-olivine–anhydrite–C system leads to the formation of low-Fe, low-Ni olivine, diopside, and pyrrhotite. During this desulfation process a reduced sulfur fluid forms according to the reaction $olivine + anhydrite + C \rightarrow diopside + S + CO_2$. The resulting fluid is a recrystallization medium for Fe,Ni-bearing olivine, extraction of Fe, Ni, and other elements and subsequent crystallization of sulfide ($Fe_{0.74-0.87}Ni_{0.09-0.16}S$) in association with pyroxene (i.e., olivine sulfidation).

As a result of the interaction in the Fe,Ni-olivine–anhydrite–C system at 1450 °C, olivine recrystallization occurs, accompanied by the formation of immiscible silicate-oxide (12.8–14.6 wt % FeO and 13.6–26.4 wt % CaO) and sulfide ($Fe_{0.66-0.89}Ni_{0.12-0.34}S$) melts. It was experimentally demonstrated that in the process of olivine recrystallization, a selective capture of inclusions of the sulfide melt takes place. It has been established that the recrystallization media for olivine are both a reduced S-rich fluid and a silicate-oxide melt with dissolved sulfur.

It is found that at 1450 °C in the Fe,Ni-olivine–Mg-sulfate–C system, olivine recrystallization occurs, accompanied by the capture of melt inclusions, generation of carbonate-silicate (15–24 wt % FeO and 6–8.5 wt % CO_2) and sulfide ($Fe_{0.70-0.87}Ni_{0.07-0.28}S$) melts, and the recrystallization of graphite in the carbonate-silicate melt. The formation of the carbonate component of the melt occurs as a result of the desulfation reaction, according to the scheme $Mg-sulfate + C \rightarrow magnesite + S$.

It was experimentally demonstrated that as a result of anhydrite- and Mg-sulfate-bearing slab desulfation, sulfide mineralization of mantle silicate rocks, crystallization of the minerals of wehrlitic assemblage—olivine and diopside, and the generation of potential agents of mantle metasomatism— SO_3 , S, CO_2 fluids, in addition to silicate-oxide melt or carbonate-silicate melt occur.

Author Contributions: Conceptualization, Y.P., Y.B. (Yuliya Bataleva) and Y.B. (Yuri Borzdov); methodology, Y.B. (Yuri Borzdov); formal analysis, Y.B. (Yuliya Bataleva); investigation, Y.B. (Yuliya Bataleva), Y.P.; writing-original draft preparation, Y.B. (Yuliya Bataleva); writing-review & editing, Y.P. and Y.B. (Yuliya Bataleva); visualization, Y.B. (Yuliya Bataleva); supervision, Y.P.

Funding: This work was supported by the Russian Science Foundation under Grant No. 14-27-00054.

Acknowledgments: The authors thank three anonymous reviewers for helpful and constructive reviews.

Conflicts of Interest: The authors declare no conflict of interest.

References

1. Alard, O.; Lorand, J.-P.; Reisberg, L.; Bodinier, J.-L.; Dautria, J.-M.; O'Reilly, S. Volatile-rich metasomatism in Montferrier xenoliths (Southern France): Implications for the abundances of chalcophile and highly siderophile elements in the subcontinental mantle. *J. Petrol.* **2011**, *52*, 2009–2045. [[CrossRef](#)]
2. Delpéch, G.; Lorand, J.P.; Grégoire, M.; Cottin, J.-Y.; O'Reilly, S.Y. In-situ geochemistry of sulfides in highly metasomatized mantle xenoliths from Kerguelen, southern Indian Ocean. *Lithos* **2012**, *154*, 296–314. [[CrossRef](#)]
3. Evans, K.A.; Powell, R. The effect of subduction on the sulphur, carbon and redox budget of lithospheric mantle. *J. Metamorph. Geol.* **2015**, *33*, 649–670. [[CrossRef](#)]
4. Zajacz, Z. The effect of melt composition on the partitioning of oxidized sulfur between silicate melts and magmatic volatiles. *Geochim. Cosmochim. Acta* **2015**, *158*, 223–244. [[CrossRef](#)]
5. Kitayama, Y.; Thomassot, E.; Galy, A.; Golovin, A.; Korsakov, A.; d'Eyrames, E.; Assayag, N.; Bouden, N.; Ionov, D. Co-magmatic sulfides and sulfates in the Udachnaya-East pipe (Siberia): A record of the redox state and isotopic composition of sulfur in kimberlites and their mantle sources. *Chem. Geol.* **2017**, *455*, 315–330. [[CrossRef](#)]
6. Alt, J.C.; Shanks, W.C.; Jackson, M.C. Cycling of sulfur in subduction zones: The geochemistry of sulfur in the Mariana-Island Arc and back-arc trough. *Earth Planet. Sci. Lett.* **1993**, *119*, 477–494. [[CrossRef](#)]
7. Evans, K.A. The redox budget of subduction zones. *Earth Sci. Rev.* **2012**, *113*, 11–32. [[CrossRef](#)]
8. Jégo, S.; Dasgupta, R. The fate of sulfur during fluid-present melting of subducting basaltic crust at variable oxygen fugacity. *J. Petrol.* **2014**, *55*, 1019–1050. [[CrossRef](#)]
9. Tomkins, A.; Evans, K.A. Separate zones of sulfate and sulfide release from subducted mafic oceanic crust. *Earth Planet. Sci. Lett.* **2015**, *428*, 73–83. [[CrossRef](#)]
10. Wirth, R.; Kaminsky, F.; Matsyuk, S.; Schreiber, A. Unusual micro- and nano-inclusions in diamonds from the Juina Area, Brazil. *Earth Planet. Sci. Lett.* **2009**, *286*, 292–303. [[CrossRef](#)]
11. Leung, I.S. Silicon carbide cluster entrapped in a diamond from Fuxian, China. *Am. Mineral.* **1990**, *65*, 1110–1119.
12. Evans, K.A.; Tomkins, A.G.; Cliff, J.; Fiorentini, M.L. Insights into subduction zone sulfur recycling from isotopic analysis of eclogite-hosted sulfides. *Chem. Geol.* **2014**, *365*, 1–19. [[CrossRef](#)]
13. Stephens, D.R. The hydrostatic compression of eight rocks. *J. Geophys. Res.* **1968**, *69*, 2967–2978. [[CrossRef](#)]
14. Borg, I.Y.; Smith, D.K. A high pressure polymorph of CaSO₄. *Contrib. Mineral. Petrol.* **1975**, *50*, 127–133. [[CrossRef](#)]
15. Langenhorst, F.; Deutsch, A.; Homeman, U.; Ivano, B.A.; Lounejeva, E. On the shock behaviour of anhydrite: Experimental results and natural observations. In Proceedings of the 34th Annual Lunar and Planetary Science Conference, League City, TX, USA, 17–21 March 2003.
16. Bradbury, S.E.; Williams, Q. X-ray diffraction and infrared spectroscopy of monazite-structured CaSO₄ at high pressures: Implications for shocked anhydrite. *J. Phys. Chem. Solids* **2009**, *70*, 134–141. [[CrossRef](#)]
17. Fujii, T.; Ohfuji, H.; Inoue, T. Phase relation of CaSO₄ at high pressure and temperature up to 90 GPa and 2300 K. *Phys. Chem. Miner.* **2016**, *43*, 353–361. [[CrossRef](#)]
18. Jégo, S.; Dasgupta, R. Fluid-present melting of sulfide-bearing ocean-crust: Experimental constraints on the transport of sulfur from subducting slab to mantle wedge. *Geochim. Cosmochim. Acta* **2013**, *110*, 106–134. [[CrossRef](#)]
19. Haggerty, S.E. Diamond genesis in a multiply-constrained model. *Nature* **1986**, *320*, 34–38. [[CrossRef](#)]
20. Sato, K.; Katsura, T. Sulfur: A new solvent-catalyst for diamond synthesis under high-pressure and high-temperature conditions. *J. Cryst. Growth* **2001**, *223*, 189–194. [[CrossRef](#)]
21. Pal'yanov, Y.N.; Borzdov, Y.M.; Kupriyanov, I.N.; Gusev, V.A.; Khokhryakov, A.F.; Sokol, A.G. High pressure synthesis and characterization of diamond from sulfur-carbon system. *Diam. Relat. Mater.* **2001**, *10*, 2145–2152. [[CrossRef](#)]
22. Palyanov, Y.N.; Kupriyanov, I.N.; Borzdov, Y.M.; Sokol, A.G.; Khokhryakov, A.F. Diamond Crystallization from a sulfur–carbon system at HPHT Conditions. *Cryst. Growth Des.* **2009**, *9*, 2922–2926. [[CrossRef](#)]
23. Kullerud, G.; Yoder, H.S., Jr. *Sulfide-Silicate Relations: Carnegie Institution of Washington Year Book*, v. 62; Carnegie Institution of Washington: Washington, DC, USA, 1963; pp. 215–218.

24. Bataleva, Y.V.; Palyanov, Y.N.; Borzdov, Y.M.; Sobolev, N.V. Sulfidation of silicate mantle by reduced S-bearing metasomatic fluids and melts. *Geology* **2016**, *44*, 271–274. [[CrossRef](#)]
25. Pal'yanov, Y.N.; Sokol, A.G.; Borzdov, Y.M.; Khokhryakov, A.F. Fluid-bearing alkaline–carbonate melts as the medium for the formation of diamonds in the Earth's mantle: An experimental study. *Lithos* **2002**, *60*, 145–159. [[CrossRef](#)]
26. Sokol, A.G.; Borzdov, Y.M.; Palyanov, Y.N.; Khokhryakov, A.F. High-temperature calibration of a multi-anvil high pressure apparatus. *High Press. Res.* **2015**, *35*, 139–147. [[CrossRef](#)]
27. Bataleva, Y.V.; Palyanov, Y.N.; Borzdov, Y.M.; Bayukov, O.A.; Zdrokov, E.V. Iron carbide as a source of carbon for graphite and diamond formation under lithospheric mantle P-T parameters. *Lithos* **2017**, *286–287*, 151–161. [[CrossRef](#)]
28. Dasgupta, R.; Buono, A.; Whelan, G.; Walker, D. High-pressure melting relations in Fe–C–S systems: Implications for formation, evolution, and structure of metallic cores in planetary bodies. *Geochim. Cosmochim. Acta* **2009**, *73*, 6678–6691. [[CrossRef](#)]
29. Palyanov, Y.N.; Borzdov, Y.M.; Bataleva, Y.V.; Sokol, A.G.; Palyanova, G.A.; Kupriyanov, I.N. Reducing role of sulfides and diamond formation in the Earth's mantle. *Earth Planet. Sci. Lett.* **2007**, *260*, 242–256. [[CrossRef](#)]
30. Cartigny, P.; Boyd, S.R.; Harris, J.W.; Javoy, M. Nitrogen isotopes in peridotitic diamonds from Fuxian, China: The mantle signature. *Terra Nova* **1997**, *9*, 175–179. [[CrossRef](#)]
31. Brazhkin, V.V.; Popova, S.V.; Voloshin, R.N. Pressure-temperature phase diagram of molten elements: Selenium, sulfur and iodine. *Phys. B Condens. Matter* **1999**, *265*, 64–71. [[CrossRef](#)]
32. Sharp, W.E. Melting curves of sphalerite, galena, and pyrrhotite and the decomposition curve of pyrite between 30 and 65 kilobars. *J. Geophys. Res.* **1969**, *74*, 1645–1652. [[CrossRef](#)]
33. Zhang, Z.; Lentsch, N.; Hirschmann, M.M. Carbon-saturated monosulfide melting in the shallow mantle: Solubility and effect on solidus. *Contrib. Mineral. Petrol.* **2015**, *170*, 47. [[CrossRef](#)]
34. Papike, J.J.; Spilde, M.N.; Fowler, G.W.; Layne, G.D.; Shearer, C.K. The Lodran primitive achondrite: Petrogenetic insights from electron and ion microprobe analysis of olivine and orthopyroxene. *Geochim. Cosmochim. Acta* **1995**, *59*, 3061–3070. [[CrossRef](#)]
35. Fleet, M.E.; MacRae, N.D. Sulfidation of Mg-rich olivine and the stability of niningerite in enstatite chondrites. *Geochim. Cosmochim. Acta* **1987**, *51*, 1511–1521. [[CrossRef](#)]
36. Zajacz, Z.; Candela, P.A.; Piccoli, P.M.; Sanchez-Valle, C.; Waelle, M. Solubility and partitioning behavior of Au, Cu, Ag and reduced S in magmas. *Geochim. Cosmochim. Acta* **2013**, *112*, 288–304. [[CrossRef](#)]
37. Kogarko, L.N.; Henderson, C.M.B.; Pacheco, H. Primary Ca-rich carbonatite magma and carbonate-silicate-sulphide liquid immiscibility in the upper mantle. *Contrib. Mineral. Petrol.* **1995**, *121*, 267–274. [[CrossRef](#)]
38. Gunn, S.C.; Luth, R.W. Carbonate reduction by Fe-S-O melts at high pressure and high temperature. *Am. Mineral.* **2006**, *91*, 1110–1116. [[CrossRef](#)]
39. Bataleva, Y.V.; Palyanov, Y.N.; Borzdov, Y.M.; Kupriyanov, I.N.; Sokol, A.G. Synthesis of diamonds with mineral, fluid and melt inclusions. *Lithos* **2016**, *265*, 292–303. [[CrossRef](#)]
40. Dasgupta, R.; Hirschmann, M.M. The deep carbon cycle and melting in Earth's interior. *Earth Planet. Sci. Lett.* **2010**, *298*, 1–13. [[CrossRef](#)]

